Organometallic Complexes for Nonlinear Optics. 43. Quadratic Optical Nonlinearities of Dipolar Alkynylruthenium Complexes with Phenyleneethynylene/Phenylenevinylene Bridges

ARTICLE *in* INORGANIC CHEMISTRY · APRIL 2009

Impact Factor: 4.76 · DOI: 10.1021/ic801953z · Source: PubMed

11 AUTHORS, INCLUDING:

Marie Cifuentes
Australian National University
173 PUBLICATIONS **2,934** CITATIONS
SEE PROFILE

Mark G Humphrey
Australian National University
338 PUBLICATIONS **6,459** CITATIONS
SEE PROFILE

Inorg. Chem. **2009**, *48*, 3562−3572

Organometallic Complexes for Nonlinear Optics. 43. Quadratic Optical Nonlinearities of Dipolar Alkynylruthenium Complexes with Phenyleneethynylene/Phenylenevinylene Bridges

Luca Rigamonti,[†,‡] Bandar Babgi,[†] Marie P. Cifuentes,[†] Rachel L. Roberts,[†] Simon Petrie,[†] Robert Stranger,[†] Stefania Righetto,[‡] Ayele Teshome,[§] Inge Asselberghs,[§] Koen Clays,[§] and Mark G. Humphrey*[,†]

Department of Chemistry, Australian National University, Canberra, ACT 0200, Australia, Dipartimento di Chimica Inorganica, Metallorganica e Analitica "L. Malatesta", Università degli Studi di Milano, via Venezian 21, 20133 Milano, Italy, and Department of Chemistry, University of Leuven, Celestijnenlaan 200D, B-3001 Leuven, Belgium

Received October 14, 2008

The syntheses of *trans*-[Ru(4,4′-C≡CC_6H_4C≡$CC_6H_4NO_2$)Cl(dppe)$_2$] (**19**) and the systematically varied complexes *trans*-[Ru(4,4′,4″-C≡$CC_6H_4X_2C_6H_4Y_2C_6H_4NO_2$)Cl($L_2$)$_2$] [$L_2$ = dppe, X_2 = C≡C, Y_2 = (*E*)-CH=CH (**12**), C≡C (**18**); L_2 = dppe, X_2 = (*E*)-CH=CH, Y_2 = C≡C (**14**), (*E*)-CH=CH (**16**); L_2 = dppm, X_2 = C≡C, Y_2 = (*E*)-CH=CH (**13**); L_2 = dppm, X_2 = (*E*)-CH=CH, Y_2 = C≡C (**15**), (*E*)-CH=CH (**17**)] are reported, the latter being donor-bridge-acceptor complexes varying in bridge composition by replacement of yne with *E*-ene linkages, together with their cyclic voltammetric data, linear optical, and quadratic nonlinear optical response data. $Ru^{II/III}$ oxidation potentials increase on replacing yne linkage by *E*-ene linkage at the phenylene adjacent to the metal center, and on replacing dppe by dppm co-ligands. The low-energy optical absorption maxima occur in the region 20400−23300 cm^{-1} and are metal-to-ligand charge-transfer (MLCT) in origin; these bands undergo a blue-shift upon π-bridge lengthening by addition of phenyleneethynylene units, and on replacing *E*-ene linkages by yne linkages. Time-dependent density functional theory calculations on model complexes have suggested assignments for the low-energy bands. The optical spectra of selected oxidized species contain low-energy ligand-to-metal charge transfer (LMCT) bands centered in the region 9760−11800 cm^{-1}. Quadratic molecular nonlinearities from hyper-Rayleigh scattering (HRS) studies at 1064 nm reveal an increase in the two-level-corrected β_0 value on π-bridge lengthening, a trend that is not seen with β values because of the blue-shift in λ_{max} for this structural modification. Replacing yne linkages by *E*-ene linkage at the phenylene adjacent to the metal center or dppm co-ligand by dppe results in an increase in β and β_0 values. In contrast, quadratic molecular nonlinearities by HRS at 1300 nm or electric field-induced second-harmonic generation (EFISH) studies at 1907 nm do not afford clear trends.

Introduction

The nonlinear optical (NLO) properties of organometallic complexes have been of considerable interest.[1−3] In many instances, structure−property relationships developed in organic systems have been propagated into the organometallic domain. For example, dipolar molecules with a donor-π-bridge-acceptor composition were found to have large quadratic NLO properties in early studies with organic compounds, and these properties could be further enhanced by specific π-bridge modification (e.g., replacing yne-linkages by *E*-ene-linkages in proceeding from end-functionalized tolanes to the corresponding *E*-stilbenes).[4] Replacing classical organic donor groups by ligated metal

* To whom correspondence should be addressed. E-mail: mark.humphrey@anu.edu.au. Phone: +61 2 6125 2927. Fax: +61 2 6125 0760.
† Australian National University.
‡ Università degli Studi di Milano.
§ University of Leuven.

(1) Long, N. J. *Angew. Chem., Int. Ed. Engl.* **1995**, *34*, 21.
(2) Verbiest, T.; Houbrechts, S.; Kauranen, M.; Clays, K.; Persoons, A. *J. Mater. Chem.* **1997**, *7*, 2175.
(3) Whittall, I. R.; McDonagh, A. M.; Humphrey, M. G.; Samoc, M. *Adv. Organomet. Chem.* **1999**, *43*, 349.
(4) Cheng, L.-T.; Tam, W.; Stevenson, S. H.; Meredith, G. R.; Rikken, G.; Marder, S. R. *J. Phys. Chem.* **1991**, *95*, 10631.

10.1021/ic801953z CCC: $40.75
Published on Web 03/19/2009

centers adds additional design flexibility, can result in enhancement of quadratic NLO response,[5−7] and in some instances introduces functionality to permit NLO switching (e.g., by reversible oxidation at the metal center).[8−17] We have previously reported selected structure-quadratic NLO activity studies for organometallic (and particularly metal alkynyl) complexes.[18−28] Almost all complexes that we have studied thus far incorporate π-bridge units containing one or two phenyl rings coupled together in various ways. When we assessed the effect of π-bridge lengthening, in proceeding from *trans*-[Ru(4-C≡C$C_6H_4NO_2$)Cl(dppm)$_2$] to *trans*-[Ru(4,4′-C≡CC_6H_4C≡C$C_6H_4NO_2$)Cl(dppm)$_2$] and then *trans*-[Ru-(4,4′,4″-C≡CC_6H_4C≡CC_6H_4C≡C$C_6H_4NO_2$)Cl(dppm)$_2$], we noted a nonlinear increase in nonlinearity [β_{1064}: 767 to 833 to 1379 (10^{-30} esu); β_0: 129 to 161 to 365 (10^{-30} esu)].[20] The last-mentioned is the only complex with a three-phenyl-ring-containing bridging ligand, but the rings are coupled together solely by ethynyl linkages. We report herein several new alkyne ligands corresponding to either specific or wholesale replacement of the arene-linking ethynyl units in 4,4′,4″-HC≡CC_6H_4C≡CC_6H_4C≡C$C_6H_4NO_2$ by *E*-ethenyl groups, the corresponding ruthenium alkynyl complex derivatives, assessment of the impact of these structural modifications on electrochemical, linear optical, spectroelectrochemical, and quadratic nonlinear optical properties, and theoretical studies directed at rationalizing our experimental observations.

Experimental Section

Materials. All reactions were performed under a nitrogen atmosphere with the use of Schlenk techniques unless otherwise stated. Dichloromethane and triethylamine were dried by distilling over calcium hydride; all other solvents were used as received. Petrol is a fraction of boiling range 60−80 °C. Chromatography was performed on silica gel or ungraded basic alumina. Ammonium hexafluorophosphate, sodium hexafluorophosphate, tetra-*n*-butylammonium fluoride, 1,3-propandiol, copper(I) iodide, sodium bicarbonate, *p*-toluenesulfonic acid, magnesium sulfate, $PdCl_2(PPh_3)_2$, $Pd(PPh_3)_4$, and DIBALH (toluene solution) (Aldrich) were used as received. Triethylphosphite (Aldrich) was distilled before use. The following were prepared by literature procedures: 4-(bromomethyl)benzaldehyde,[29] 4-Me_3SiC≡CC_6H_4I,[30] 4-Me_3SiC≡CC_6H_4Br, 4-HC≡C$C_6H_4NO_2$,[31] 4-Me_3SiC≡CC_6H_4CHO, 4-HC≡CC_6H_4CHO,[32] 4-HC≡CC_6H_4CHO(CH_2)$_3$O,[33] (*E*)-4,4′-HC≡CC_6H_4CH=CH$C_6H_4NO_2$,[20] 4-(EtO)$_2$(O)PC$H_2C_6H_4$I,[34] 4-(EtO)$_2$(O)PC$H_2C_6H_4NO_2$,[20] 4,4′-HC≡CC_6H_4C≡C$C_6H_4NO_2$,[35] 4,4′,4″-HC≡CC_6H_4C≡CC_6H_4C≡C$C_6H_4NO_2$,[20] *cis*-[$RuCl_2$(dppe)$_2$], *cis*-[$RuCl_2$(dppm)$_2$],[36] *trans*-[Ru(4-C≡C$C_6H_4NO_2$)Cl(dppe)$_2$] (**20**),[37] *trans*-[Ru{(*E*)-4,4′-C≡C-C_6H_4CH=CH$C_6H_4NO_2$}Cl(dppe)$_2$] (**21**),[20] *trans*-[Ru(4-C≡CC_6H_4-NO_2)Cl(dppm)$_2$] (**22**), *trans*-[Ru{(*E*)-4,4′-C≡CC_6H_4CH=CHC_6H_4-NO_2}Cl(dppm)$_2$] (**23**),[27] *trans*-[Ru(4,4′-C≡CC_6H_4C≡C$C_6H_4NO_2$)-Cl(dppm)$_2$] (**24**), *trans*-[Ru(4,4′,4″-C≡CC_6H_4C≡CC_6H_4C≡CC_6H_4-NO_2)Cl(dppm)$_2$] (**25**).[20] The syntheses of **1**−**11** are given in the Supporting Information.

Methods and Instrumentation. Microanalyses were carried out at the Australian National University. UV−vis spectra of solutions in 1 cm quartz cells were recorded using a Cary 5 spectrophotometer; bands are reported as frequency (cm^{-1}) [extinction coefficient (10^4 M^{-1} cm^{-1})]. Infrared spectra were recorded as either KBr discs or dichloromethane solutions using a Perkin-Elmer System 2000 FT-IR; peaks are reported in cm^{-1}. ^{1}H (300 MHz), ^{13}C (75 MHz), and ^{31}P (121 MHz) NMR spectra were recorded using a Varian Gemini-300 FT NMR spectrometer and are referenced to residual chloroform (7.26 ppm), $CDCl_3$ (77.0 ppm), or external H_3PO_4 (0.0 ppm), respectively; atom labeling follows the numbering scheme in Chart S1, Supporting Information. Electrospray ionization (ESI) mass spectra were recorded using a Water's/Micromass LC/ZMD

(5) Whittall, I. R.; McDonagh, A. M.; Humphrey, M. G.; Samoc, M. *Adv. Organomet. Chem.* **1998**, *42*, 291.
(6) Heck, J.; Dabek, S.; Meyer-Friedrichsen, T.; Wong, H. *Coord. Chem. Rev.* **1999**, *190−192*, 1217.
(7) Morrall, J. P.; Dalton, G. T.; Humphrey, M. G.; Samoc, M. *Adv. Organomet. Chem.* **2007**, *55*, 61.
(8) Coe, B. J. *Chem.−Eur. J.* **1999**, *5*, 2464.
(9) Delaire, J. A.; Nakatani, K. *Chem. Rev.* **2000**, *100*, 1817.
(10) Weyland, T.; Ledoux, I.; Brasselet, S.; Zyss, J.; Lapinte, C. *Organometallics* **2000**, *19*, 5235.
(11) Cifuentes, M. P.; Powell, C. E.; Humphrey, M. G.; Heath, G. A.; Samoc, M.; Luther-Davies, B. *J. Phys. Chem. A* **2001**, *105*, 9625.
(12) Malaun, M.; Reeves, Z. R.; Paul, R. L.; Jeffery, J. C.; McCleverty, J. A.; Ward, M. D.; Asselberghs, I.; Clays, K.; Persoons, A. *Chem. Commun.* **2001**, 49.
(13) Powell, C. E.; Cifuentes, M. P.; Morrall, J. P. L.; Stranger, R.; Humphrey, M. G.; Samoc, M.; Luther-Davies, B.; Heath, G. A. *J. Am. Chem. Soc.* **2003**, *125*, 602.
(14) Powell, C. E.; Humphrey, M. G.; Cifuentes, M. P.; Morrall, J. P.; Samoc, M.; Luther-Davies, B. *J. Phys. Chem. A* **2003**, *107*, 11264.
(15) Asselberghs, I.; Clays, K.; Persoons, A.; McDonagh, A. M.; Ward, M. D.; McCleverty, J. *Chem. Phys. Lett.* **2003**, *368*, 408.
(16) Paul, F.; Costuas, K.; Ledoux, I.; Deveau, S.; Zyss, J.; Halet, J.-F.; Lapinte, C. *Organometallics* **2002**, *21*, 5229.
(17) Cifuentes, M. P.; Humphrey, M. G.; Morrall, J. P.; Samoc, M.; Paul, F.; Lapinte, C.; Roisnel, T. *Organometallics* **2005**, *24*, 4280.
(18) Powell, C. E.; Humphrey, M. G. *Coord. Chem. Rev.* **2004**, *248*, 725.
(19) Cifuentes, M. P.; Humphrey, M. G. *J. Organomet. Chem.* **2004**, *689*, 3968.
(20) Hurst, S.; Cifuentes, M. P.; Morrall, J. P. L.; Lucas, N. T.; Whittall, I. R.; Humphrey, M. G.; Asselberghs, I.; Persoons, A.; Samoc, M.; Luther-Davies, B.; Willis, A. C. *Organometallics* **2001**, *20*, 4664.
(21) Whittall, I. R.; Humphrey, M. G.; Houbrechts, S.; Persoons, A.; Hockless, D. C. R. *Organometallics* **1996**, *15*, 5738.
(22) Whittall, I. R.; Cifuentes, M. P.; Humphrey, M. G.; Luther-Davies, B.; Samoc, M.; Houbrechts, S.; Persoons, A.; Heath, G. A.; Hockless, D. C. R. *J. Organomet. Chem.* **1997**, *549*, 127.
(23) Naulty, R. H.; McDonagh, A. M.; Whittall, I. R.; Cifuentes, M. P.; Humphrey, M. G.; Houbrechts, S.; Maes, J.; Persoons, A.; Heath, G. A.; Hockless, D. C. R. *J. Organomet. Chem.* **1998**, *563*, 137.
(24) McDonagh, A. M.; Cifuentes, M. P.; Lucas, N. T.; Humphrey, M. G.; Houbrechts, S.; Persoons, A. *J. Organomet. Chem.* **2000**, *605*, 193.
(25) Whittall, I. R.; Cifuentes, M. P.; Humphrey, M. G.; Luther-Davies, B.; Samoc, M.; Houbrechts, S.; Persoons, A.; Heath, G. A.; Bogsanyi, D. *Organometallics* **1997**, *16*, 2631.
(26) Whittall, I. R.; Humphrey, M. G.; Hockless, D. C. R.; Skelton, B. W.; White, A. H. *Organometallics* **1995**, *14*, 3970.
(27) McDonagh, A. M.; Whittall, I. R.; Humphrey, M. G.; Skelton, B. W.; White, A. H. *J. Organomet. Chem.* **1996**, *519*, 229.
(28) Naulty, R. H.; Cifuentes, M. P.; Humphrey, M. G.; Houbrechts, S.; Boutton, C.; Persoons, A.; Heath, G. A.; Hockless, D. C. R.; Luther-Davies, B.; Samoc, M. *J. Chem. Soc., Dalton Trans.* **1997**, 4167.
(29) Meier, H.; Holst, H.; Oehlhof, A. *Eur. J. Org. Chem.* **2003**, 4173.
(30) Hsung, P.; Chidsey, C. E. D.; Sita, L. R. *Organometallics* **1995**, *14*, 4808.
(31) Takahashi, S.; Kuroyama, Y.; Sonogashira, K.; Hagihara, N. *Synthesis* **1980**, 627.
(32) Austin, W. B.; Bilow, N.; Kelleghan, W. J.; Lau, K. S. Y. *J. Org. Chem.* **1981**, *46*, 2280.
(33) The general 1,3-dioxane synthesis is described in: Green, T. W.; Wuts, P. G. M. *Protective Groups in Organic Synthesis*; Wiley-Interscience: New York, 1999; Vols. *308−322*, pp 724−727.
(34) Kung, H.; Lee, C.-W.; Zhuang, Z.-P.; Kung, M.-P.; Hou, C.; Ploessl, K. *J. Am. Chem. Soc.* **2001**, *123*, 12740.
(35) Lavastre, O.; Cabioch, S.; Dixneuf, P. H.; Vohlidal, J. *Tetrahedron* **1997**, *53*, 7595.
(36) Chaudret, B.; Commenges, G.; Poilblanc, R. *J. Chem. Soc., Dalton Trans.* **1984**, 1635.
(37) Touchard, D.; Haquette, P.; Guesmi, S.; Pichon, L. L.; Daridor, A.; Toupet, L.; Dixneuf, P. H. *Organometallics* **1997**, *16*, 3640.

single quadrupole liquid chromatograph-MS, high resolution ESI mass spectra were carried out utilizing a Bruker Apex 4.7T FTICR-MS instrument, and EI mass spectra were recorded using a VG Quattro II triple quadrupole MS; all mass spectrometry peaks are reported as *m*/*z* (assignment, relative intensity). Cyclic voltammetry measurements were recorded using a MacLab 400 interface and MacLab potentiostat from ADInstruments. Measurements were carried out at room temperature using Pt disk working-, Pt wire auxiliary-, and Ag/AgCl reference electrodes, such that the ferrocene/ferrocenium redox couple was located at 0.56 V (peak separation ca. 0.09 V). Scan rates were typically 100 mV s^{-1}. Electrochemical solutions contained 0.1 M $(NBu^n_4)PF_6$ and about 10^{-3} M complex in dichloromethane. Solutions were purged and maintained under a nitrogen atmosphere. Electronic spectra were recorded using a Cary 5 spectrophotometer. Solution spectra of the oxidized species were obtained at 298 K by electrogeneration in an optically transparent thin-layer electrochemical cell with potentials about 300 mV beyond $E_{1/2}$ for each couple, to ensure complete electrolysis; solutions were made up in 0.3 M $(NBu^n_4)PF_6$ in dichloromethane.

Synthesis of *trans*-[Ru{(*E*)-4,4′,4″-C≡CC$_6$H$_4$C≡CC$_6$H$_4$CH=CHC$_6$H$_4$NO$_2$}Cl(dppe)$_2$](12). *cis*-[RuCl$_2$(dppe)$_2$] (357 mg, 0.37 mmol) and NH_4PF_6 (67 mg, 0.41 mmol) were added to a suspension of **4** (130 mg, 0.37 mmol) in CH_2Cl_2 (50 mL). The orange mixture was stirred at room temperature overnight. NEt_3 (1 mL) was added, and the red mixture stirred at room temperature for 2 h. The reaction mixture was purified by column chromatography on alumina, eluting with CH_2Cl_2/petrol/NEt_3 (10:10:1). Reduction in volume of the solvent on a rotary evaporator afforded **12** as a red powder (280 mg, 60%). ESI MS: 1247 ($[M - Cl]^+$, 75), 898 ($[Ru(dppe)_2]^+$, 10). Anal. Calcd for $C_{76}H_{62}ClNO_2P_4Ru \cdot 1.5CH_2Cl_2$: C, 66.06; H, 4.65; N, 1.00. Found: C, 65.88; H, 4.91; N, 1.19. UV−vis (CH_2Cl_2): 22200 sh [3.0], 26400 [6.1], 40400 sh [5.4]. IR (CH_2Cl_2): 2062 ν(RuC≡C). ^{1}H NMR: δ 2.69 (m, 8H, PCH_2), 5.28 (s, 3H, CH_2Cl_2), 6.56 (d, J_{HH} = 8 Hz, 2H, H_4), 6.90−7.60 (m, 48H, H_5, H_{10}, H_{11}, H_{13}, H_{14} and Ph), 7.65 (d, J_{HH} = 9 Hz, 2H, H_{16}), 8.24 (d, J_{HH} = 9 Hz, 2H, H_{17}). ^{13}C NMR: δ 30.6 (CH_2), 84.8 (C_8), 124.3 (C_{17}), 126.8 (C_{11}), 127.1 (d, J_{CP} = 12 Hz), 128.9, 134.3 (d, J_{CP} = 16 Hz), 135.9 (m) (PPh), 131.9 (C_4, C_5), 132.7 (C_{10}), 143.7 (C_{15}), 146.9 (C_{18}), C_2, C_7, C_1 not observed. ^{31}P NMR: δ 49.7. The syntheses of **13**−**19** are similar and are given in the Supporting Information.

HRS Measurements. For studies at 1064 nm, an injection seeded Nd:YAG laser (Q-switched Nd:YAG Quanta Ray GCR, 1064 nm, 8 ns pulses, 10 Hz) was focused into a cylindrical cell (7 mL) containing the sample. The intensity of the incident beam was varied by rotation of a half-wave plate placed between crossed polarizers. Part of the laser pulse was sampled by a photodiode to measure the vertically polarized incident light intensity. The frequency-doubled light was collected by an efficient condenser system and detected by a photomultiplier. The harmonic scattering and linear scattering were distinguished by appropriate filters; gated integrators were used to obtain intensities of the incident and harmonic scattered light. The absence of a luminescence contribution to the harmonic signal was confirmed by using interference filters at different wavelengths near 532 nm. All measurements were performed in tetrahydrofuran (thf) using *p*-nitroaniline ($\beta = 21.4 \times 10^{-30}$ esu)[38] as a reference. Solutions were sufficiently dilute that absorption of scattered light was negligible.

For studies at 1300 nm, a Tsunami-pumped OPAL (model Spectra-Physics) was used. With a high repetition rate of the laser, high frequency demodulation of fluorescence contributions can be effected, a full description being given in ref 39. All measurements were performed in tetrahydrofuran using Disperse Red 1 (DR1, $\beta = 54 \times 10^{-30}$ esu in chloroform) as a reference. Experiments utilized low chromophore concentrations, the linearity of the HRS signal as a function of the chromophore concentration confirming that no significant self-absorption of the SHG signal occurred.

EFISH Measurements. The molecular NLO responses were measured by the solution-phase direct current electric-field-induced second-harmonic (EFISH) generation method[40−42] which provides γ_{EFISH} through

$$\gamma_{EFISH} = (\mu\beta_\lambda/5kT) + \gamma(-2\omega;\omega,\omega,0)$$

where $\mu\beta_\lambda/5kT$ is the dipolar orientational contribution, λ is the fundamental wavelength of the incident photon in the EFISH experiment, $\gamma(-2\omega;\omega,\omega,0)$ is the cubic electronic contribution to γ_{EFISH} which can be considered negligible for the kinds of dipolar molecules investigated here, and β_λ is the projection along the dipole moment axis of the vectorial component of the quadratic hyperpolarizability tensor, hereafter called β_{vec}. EFISH measurements were carried out in $CHCl_3$ solutions working at the non-resonant incident wavelength of 1.907 μm, using a Q-switched, mode-locked Nd:YAG laser, manufactured by Atalaser, equipped with a Raman shifter; the apparatus for the EFISH measurements was made by SOPRA (France).

Theoretical Studies. Calculations were performed using the Amsterdam Density Functional (ADF) package ADF2004.01,[43] developed by Baerends et al.[44,45] These calculations were undertaken to characterize the lowest-frequency-allowed single-photon transitions of a set of model compounds containing the unsaturated hydrocarbon bridges of compounds **12** to **18**. These models were of the form $[Ru]C_2C_6H_4C_2H_iC_6H_4C_2H_jC_6H_4NO_2$ ([Ru] = *trans*-$RuCl(PH_2CH_2PH_2)_2$; $i = 0, 2, j = 0, 2$). In the theoretical discussion, the models are denoted as **12M**, **14M**, **16M**, and **18M** to indicate the laboratory compounds of which they are structural homologues. Symmetry was constrained as either C_{2v} (**18M**) or C_s (**12M**, **14M**, **16M**) as appropriate. In all calculations and for all atoms, the Slater-type orbital basis sets used were of triple-ζ-plus-polarization quality (TZP). Electrons in orbitals up to and including 1s {C}, 2p {P, Cl}, and 4p {Ru} were treated in accordance with the frozen-core approximation. Geometry optimizations employed the gradient algorithm of Versluis and Ziegler.[46] Functionals used in the optimization calculations were the local density approximation (LDA) to the exchange potential,[47] the correlation potential of Vosko, Wilk, and Nusair (VWN),[48] and the nonlocal corrections of Perdew, Burke, and Enzerhof (PBE).[49] Following optimization of the model compounds, time-dependent density functional theory

(38) Stähelin, M.; Burland, D. M.; Rice, J. E. *Chem. Phys. Lett.* **1992**, *191*, 245.
(39) Olbrechts, G.; Wostyn, K.; Clays, K.; Persoons, A. *Opt. Lett.* **1999**, 403.
(40) Levine, B.; Bethea, C. *Appl. Phys. Lett.* **1974**, *24*, 455.
(41) Singer, K. D.; Garito, A. F. *J. Chem. Phys.* **1981**, *75*, 3572.
(42) Ledoux, I.; Zyss, J. *J. Chem. Phys.* **1982**, *73*, 203.
(43) Baerends, E. J. et al. *Amsterdam Density Functional (ADF) package ADF2004.01*; Theoretical Chemistry, Vrije Universiteit: Amsterdam, The Netherlands, 2006; http://www.scm.com.
(44) Fonseca Guerra, C. F.; Snijders, J. G.; te Velde, G.; Baerends, E. J. *Theor. Chem. Acc.* **1998**, *99*, 391.
(45) te Velde, G.; Bickelhaupt, F. M.; Baerends, E. J.; Guerra, C. F.; van Gisbergen, S. J. A.; Snijders, J. G.; Ziegler, T. *J. Comput. Chem.* **2001**, *22*, 931.
(46) Versluis, L.; Ziegler, T. *J. Chem. Phys.* **1988**, *88*, 322.
(47) Parr, R. G.; Yang, W. *Density Functional Theory of Atoms and Molecules*; Oxford University Press: New York, 1989.
(48) Vosko, S. H.; Wilk, L.; Nusair, M. *Can. J. Phys* **1980**, *58*, 1200.
(49) Perdew, J. P.; Burke, K.; Ernzerhof, M. *Phys. Rev. Lett.* **1996**, *77*, 3865.

Scheme 1. Syntheses of **1**−**4**[a]

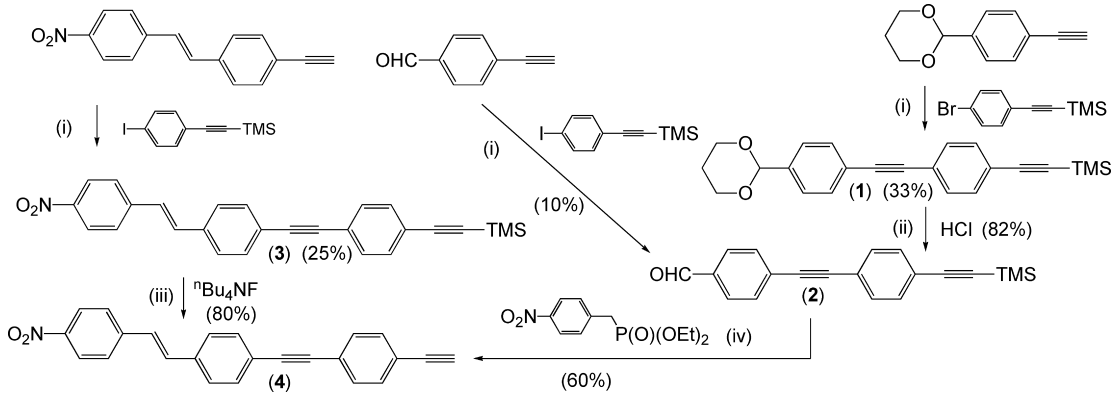

[a] (i) $PdCl_2(PPh_3)_2$ (cat.), CuI (cat.), NEt_3. (ii) Acetone. (iii) CH_2Cl_2, THF. (iv) NaOMe, THF, then H_2O, MeOH.

Scheme 2. Syntheses of **5** and **6**[a]

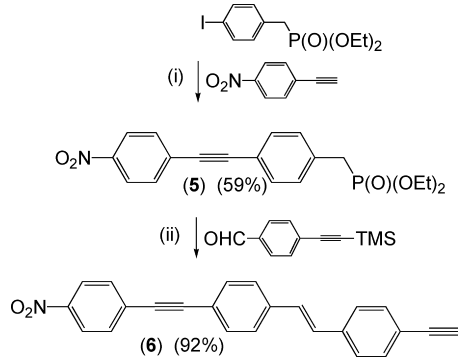

[a] (i) $Pd(PPh_3)_4$ (cat.), NEt_3. (ii) NaOMe, THF, then H_2O, MeOH.

(TD-DFT) calculations were pursued using either PBE or the asymptotically correct functional of van Leeuwen and Baerends (LB94).

Dipole moments for the model compounds were also obtained: these are listed in Table 5, and were used in combination with experimental $\mu\cdot\beta$ data to afford β_{EFISH} values.

Results

Synthesis and Characterization of Alkynes and Alkynyl Complexes. The acetylenes required for the alkynyl complex syntheses were prepared by extensions of established organic synthetic procedures (Schemes 1−3). We have previously reported the synthesis of (*E*)-4,4′-HC≡CC_6H_4CH=$CHC_6H_4NO_2$.[20] Coupling this alkyne with 4-iodo(trimethylsilylethynyl)benzene under Sonogashira conditions afforded (*E*)-4,4′,4″-$Me_3SiC{\equiv}CC_6H_4C{\equiv}CC_6H_4CH{=}CHC_6H_4NO_2$ (**3**), which could be desilylated with tetra-*n*-butylammonium fluoride to give (*E*)-4,4′,4″-HC≡$CC_6H_4C{\equiv}CC_6H_4CH{=}CHC_6H_4NO_2$ (**4**) (Scheme 1). In search of an improved synthesis, we targeted 4,4′-$Me_3SiC{\equiv}CC_6H_4C{\equiv}CC_6H_4CHO$ (**2**) as a precursor to **4**. Reacting 4-ethynylbenzaldehyde with 4-iodo(trimethylsilylethynyl)benzene under Sonogashira conditions gave **2** in very low yield and was not pursued further. Reacting 4-HC≡$CC_6H_4CHO(CH_2)_3O$ with 4-bromo(trimethylsilylethynyl)benzene, again using Sonogashira conditions, afforded 4,4′-$Me_3SiC{\equiv}CC_6H_4C{\equiv}CC_6H_4CHO(CH_2)_3O$ (**1**). The acetal protecting group was removed on reaction with acid, to afford **2**. Emmons−Horner−Wadsworth coupling of **2** with 4-$(EtO)_2(O)PCH_2C_6H_4NO_2$ proceeded with simultaneous desilylation to give **4** directly in excellent yield.

Sonogashira coupling of 4-HC≡$CC_6H_4NO_2$ and 4-$(EtO)_2$-$(O)PCH_2C_6H_4I$ afforded 4,4′-$(EtO)_2(O)PCH_2C_6H_4C{\equiv}CC_6H_4$-$NO_2$ (**5**), subsequent Emmons−Horner coupling and simultaneous desilylation giving (*E*)-4,4′,4″-HC≡$CC_6H_4CH{=}$ $CHC_6H_4C{\equiv}CC_6H_4NO_2$ (**6**) (Scheme 2). The aldehyde functionality in 4-$BrCH_2C_6H_4CHO$ was protected as the acetal 4-$BrCH_2C_6H_4CHO(CH_2)_3O$ (**7**) by reaction with 1,3-propandiol, a subsequent Arbuzov reaction giving 4-$(EtO)_2(O)PCH_2$-$C_6H_4CHO(CH_2)_3O$ (**8**) (Scheme 3). Emmons−Horner coupling of **8** with 4-$Me_3SiC{\equiv}CC_6H_4CHO$ afforded (*E*)-4,4′-HC≡$CC_6H_4CH{=}CHC_6H_4CHO(CH_2)_3O$ (**9**) in 54% yield. The acetal protecting group in **9** was removed by reaction with HCl, affording (*E*)-4,4′-HC≡$CC_6H_4CH{=}CHC_6H_4CHO$ (**10**) in excellent yield. A further Emmons−Horner coupling [**10** with 4-$(EtO)_2(O)PCH_2C_6H_4NO_2$] afforded (*E,E*)-4,4′,4″-HC≡$CC_6H_4CH{=}CHC_6H_4CH{=}CHC_6H_4NO_2$ (**11**).

The synthetic methodology employed for the preparation of the new alkynyl complexes (Scheme 4) has been successfully employed for the synthesis of related (chloro)bis(diphosphine)ruthenium complexes by several groups.[27,37,46,50−60] The new complexes **12**−**19** were characterized by IR, ^1H, ^{13}C, and ^{31}P NMR spectroscopy and ESI mass spectrometry. IR spectra contain characteristic ν(C≡C) bands at 2056−2067 cm^{-1} for the metal-bound alkynyl group, while the ^{31}P NMR spectra

(50) Hodge, A. J.; Ingham, S. L.; Kakkar, A. K.; Khan, M. S.; Lewis, J.; Long, N. J.; Parker, D. G.; Raithby, P. R. *J. Organomet. Chem.* **1995**, *488*, 205.
(51) Touchard, D.; Haquette, P.; Pirio, N.; Toupet, L.; Dixneuf, P. H. *Organometallics* **1993**, *12*, 3132.
(52) Ge, Q.; Hor, T. *Dalton Trans.* **2008**, 2929.
(53) Fondum, T. N.; Green, K. A.; Randles, M. D.; Cifuentes, M. P.; Willis, A. C.; Teshome, A.; Asselberghs, I.; Clays, K.; Humphrey, M. G. *J. Organomet. Chem.* **2008**, *693*, 1605.
(54) Gauthier, N.; Olivier, C.; Rigaut, S.; Touchard, D.; Roisnel, T.; Humphrey, M. G.; Paul, F. *Organometallics* **2008**, *27*, 1063.
(55) Fillaut, J.-L.; Andries, J.; Marwaha, R. D.; Lanoe, P.-H.; Lohio, O.; Toupet, L.; Williams, J. A. G. *J. Organomet. Chem.* **2008**, *693*, 228.
(56) Onitsuka, K.; Ohara, N.; Takei, F.; Takahashi, S. *Dalton Trans.* **2006**, 3693.
(57) Lavastre, O.; Fiedler, J. *Organometallics* **2006**, *25*, 635.
(58) Wong, W.-Y.; Wong, C.-K.; Lu, G.-L. *J. Organomet. Chem.* **2003**, *671*, 27.
(59) Rigaut, S.; Perruchon, J.; Le Pichon, L.; Touchard, D.; Dixneuf, P. H. *J. Organomet. Chem.* **2003**, *670*, 37.
(60) Fillaut, J.-L.; Perruchon, J. *Inorg. Chem. Commun.* **2002**, *5*, 1048.

Scheme 3. Syntheses of **7**−**11**[a]

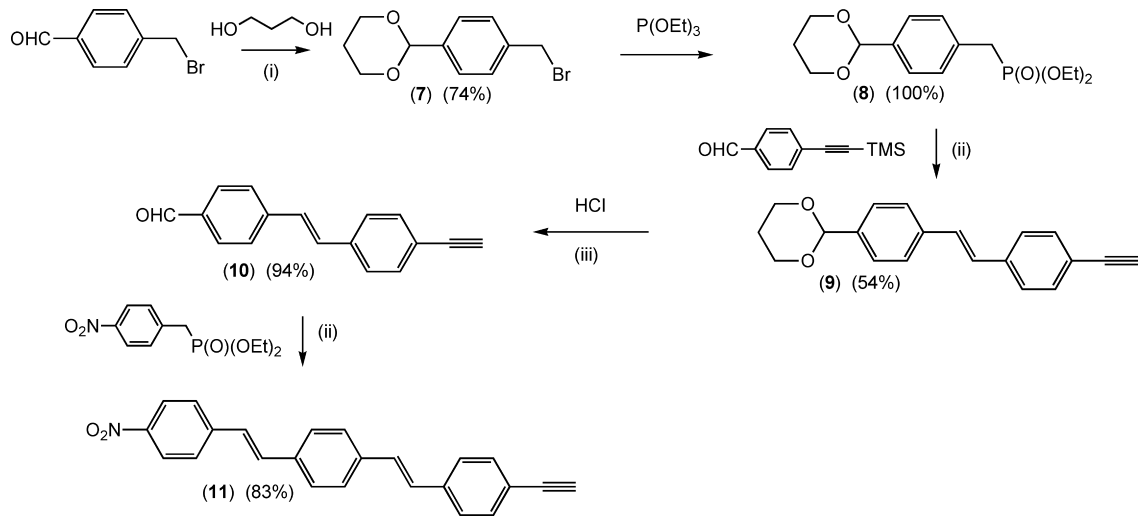

[a] (i) 4-$MeC_6H_4SO_3H$ (cat.), toluene. (ii) NaOMe, THF, then H_2O, MeOH. (iii) Acetone.

Scheme 4. Syntheses of **12**−**19**

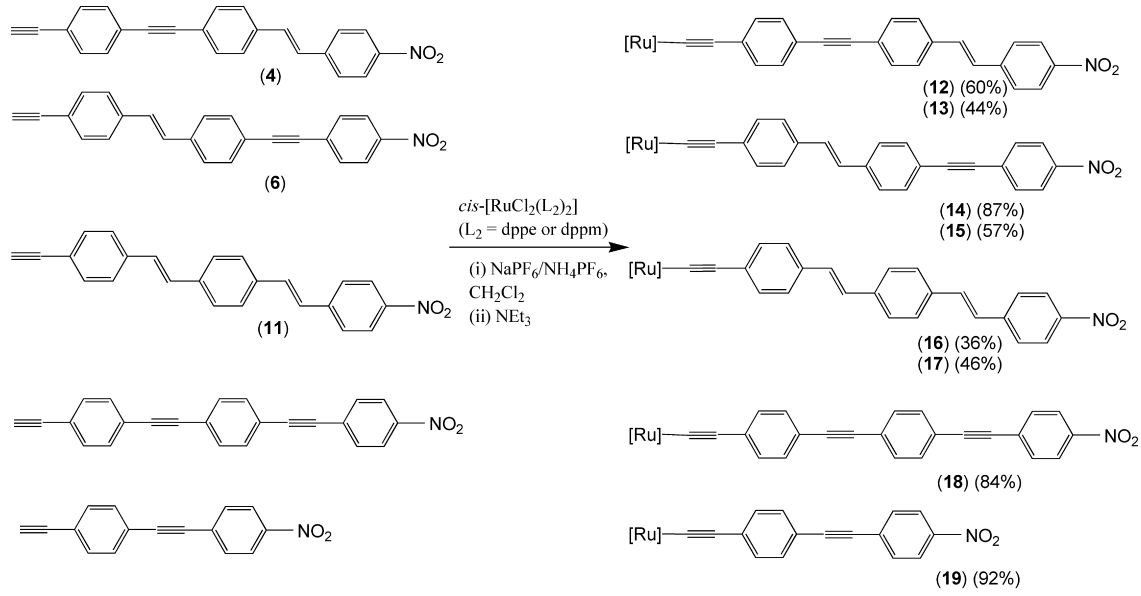

[Ru] = *trans*-$RuCl(dppe)_2$ (**12**, **14**, **16**, **18**, **19**)
[Ru] = *trans*-$RuCl(dppm)_2$ (**13**, **15**, **17**)

contain one singlet resonance each at 49.7−50.0 ppm (dppe-containing complexes) or −5.4 to −5.9 ppm (dppm-containing complexes), consistent with *trans*-disposed diphosphine ligands.

Electrochemical and Linear Optical Studies. The electrochemical properties of *trans*-bis(bidentate diphosphine)ruthenium monoalkynyl complexes,[11,13,14,20,23,24,54,56,58,59,61−85] and the related bis-alkynyl complexes[13,45,54,56,62−64,70,77,80,82−94] have attracted considerable interest recently. The results of cyclic voltammetric studies of the new ruthenium alkynyl complexes are collected in Table 1, together with data from related complexes.

The cyclic voltammograms (CVs) of complexes **12**−**25** contain a reversible or quasi-reversible anodic wave assigned

(61) Hurst, S. K.; Lucas, N. T.; Humphrey, M. G.; Asselberghs, I.; Van Boxel, R.; Persoons, A. *Aust. J. Chem.* **2001**, *54*, 447.
(62) Zuo, J.-L.; Herdtweck, E.; Fabrizi de Biani, F.; Santos, A. M.; Kühn, F. E. *New J. Chem.* **2002**, *2*, 889.
(63) Morrall, J. P.; Cifuentes, M. P.; Humphrey, M. G.; Kellens, R. D. C.; Robijns, E.; Asselbergh, I.; Clays, K.; Persoons, A.; Samoc, M.; Willis, A. C. *Inorg. Chim. Acta* **2006**, *359*, 998.
(64) Hurst, S. K.; Lucas, N. T.; Humphrey, M. G.; Isoshima, T.; Wostyn, K.; Asselberghs, I.; Clays, K.; Persoons, A.; Samoc, M.; Luther-Davies, B. *Inorg. Chim. Acta* **2003**, *350*, 62.
(65) Fillaut, J.-L.; Dua, N. N.; Geneste, F.; Toupet, L.; Sinbandhit, S. *J. Organomet. Chem.* **2006**, *91*, 5610.
(66) McDonagh, A. M.; Lucas, N. T.; Cifuentes, M. P.; Humphrey, M. G.; Houbrechts, S.; Persoons, A. *J. Organomet. Chem.* **2000**, *605*, 184.
(67) McDonagh, A. M.; Cifuentes, M. P.; Humphrey, M. G.; Houbrechts, S.; Maes, J.; Persoons, A.; Samoc, M.; Luther-Davies, B. *J. Organomet. Chem.* **2000**, *610*, 71.
(68) Wong, W.-Y.; Ho, K.-Y.; Ho, S.-L.; Lin, Z. *J. Organomet. Chem.* **2003**, *683*, 341.
(69) Hurst, S. K.; Cifuentes, M. P.; McDonagh, A. M.; Humphrey, M. G.; Samoc, M.; Luther-Davies, B.; Asselberghs, I.; Persoons, A. *J. Organomet. Chem.* **2002**, *642*, 259.

Table 1. Cyclic Voltammetric Data for Complexes **12**−**25**[a]

complex	E^0_{ox} (V) [i_{pc}/i_{pa}], $Ru^{II/III}$	E^0_{red} (V) [i_{pc}/i_{pa}], $NO_2^{0/-1}$	ref
trans-[Ru(4-C≡$CC_6H_4NO_2$)Cl(dppe)$_2$] (**20**)	0.74 [0.9]	−0.84 [0.8]	20
trans-[Ru{(*E*)-4,4′-C≡CC_6H_4CH=$CHC_6H_4NO_2$}Cl(dppe)$_2$] (**21**)	0.55 [1]	−0.98 [1]	20
trans-[Ru(4,4′-C≡CC_6H_4C≡$CC_6H_4NO_2$)Cl(dppe)$_2$] (**19**)	0.60 [1]	−0.94 [0.9]	this work
trans-[Ru{(*E*)-4,4′,4″-C≡CC_6H_4C≡CC_6H_4CH=$CHC_6H_4NO_2$}Cl(dppe)$_2$] (**12**)	0.57 [1]	−0.96 [0.9]	this work
trans-[Ru{(*E*)-4,4′,4″-C≡CC_6H_4CH=CHC_6H_4C≡$CC_6H_4NO_2$}Cl(dppe)$_2$] (**14**)	0.53 [1]	−0.92 [0.9]	this work
trans-[Ru{(*E,E*)-4,4′,4″-C≡CC_6H_4CH=CHC_6H_4CH=$CHC_6H_4NO_2$}Cl(dppe)$_2$] (**16**)	0.54 [1]	−0.91 [0.9]	this work
trans-[Ru(4,4′,4″-C≡CC_6H_4C≡CC_6H_4C≡$CC_6H_4NO_2$)Cl(dppe)$_2$] (**18**)	0.58 [1]	−0.91 [0.9]	this work
trans-[Ru(4-C≡$CC_6H_4NO_2$)Cl(dppm)$_2$] (**22**)	0.72 [1]	−0.81 [0.7]	20
trans-[Ru{(*E*)-4,4′-C≡CC_6H_4CH=$CHC_6H_4NO_2$}Cl(dppm)$_2$] (**23**)	0.56 [1]	−0.87 [0.4]	23
trans-[Ru(4,4′-C≡CC_6H_4C≡$CC_6H_4NO_2$)Cl(dppm)$_2$] (**24**)	0.57 [0.9]	−0.90 [0.7]	20
trans-[Ru{(*E*)-4,4′,4″-C≡CC_6H_4C≡CC_6H_4CH=$CHC_6H_4NO_2$}Cl(dppm)$_2$] (**13**)	0.54 [1]	−0.94 [0.9]	this work
trans-[Ru{(*E*)-4,4′,4″-C≡CC_6H_4CH=CHC_6H_4C≡$CC_6H_4NO_2$}Cl(dppm)$_2$] (**15**)	0.49 [1]	−0.92 [0.9]	this work
trans-[Ru{(*E,E*)-4,4′,4″-C≡CC_6H_4CH=CHC_6H_4CH=$CHC_6H_4NO_2$}Cl(dppm)$_2$] (**17**)	0.49 [1]	−0.97 [0.9]	this work
trans-[Ru(4,4′,4″-C≡CC_6H_4C≡CC_6H_4C≡$CC_6H_4NO_2$)Cl(dppm)$_2$] (**25**)	0.54 [1]	−0.86 [0.9]	20

[a] Conditions: CH_2Cl_2; Pt-wire auxiliary, Pt working, and Ag/AgCl reference electrodes; ferrocene/ferrocenium couple located at 0.56 V.

Table 2. Experimental Linear Optical and Hyper-Rayleigh Scattering-Derived Nonlinear Optical Response Parameters[a]

complex	λ_{max} (nm) (ε, 10^4 M^{-1} cm^{-1})	β_{1064} (10^{-30} esu)	β_0 (10^{-30} esu)[b]	β_{1300} (10^{-30} esu)	β_0 (10^{-30} esu)[c]	ref
trans-[Ru(4-C≡$CC_6H_4NO_2$)Cl(dppe)$_2$] (**20**)	477 (2.0)	351 ± 35	55			20
		562 ± 9	88 ± 1			this work
trans-[Ru{(*E*)-4,4′-C≡CC_6H_4CH=$CHC_6H_4NO_2$}Cl(dppe)$_2$] (**21**)	489 (2.6)	2676 ± 270	342			20
				140 ± 5	52 ± 5	this work
trans-[Ru(4,4′-C≡CC_6H_4C≡$CC_6H_4NO_2$)Cl(dppe)$_2$] (**19**)	468 (1.8)	1240 ± 110	225 ± 20	64 ± 3	27 ± 1	this work
trans-[Ru{(*E*)-4,4′,4″-C≡CC_6H_4C≡CC_6H_4CH=$CHC_6H_4NO_2$}Cl(dppe)$_2$] (**12**)	448 (2.5)	1800 ± 180	430	80	38	this work
trans-[Ru{(*E*)-4,4′,4″-C≡CC_6H_4CH=CHC_6H_4C≡$CC_6H_4NO_2$}Cl(dppe)$_2$] (**14**)	459 (3.5)	2800 ± 280	580	90	40	this work
trans-[Ru{(*E,E*)-4,4′,4″-C≡CC_6H_4CH=CHC_6H_4CH=$CHC_6H_4NO_2$}Cl(dppe)$_2$] (**16**)	468 (1.6)	2525 ± 175	460 ± 32	80 ± 4	34 ± 2	this work
trans-[Ru(4,4′,4″-C≡CC_6H_4C≡CC_6H_4C≡$CC_6H_4NO_2$)Cl(dppe)$_2$] (**18**)	429 (2.3)	1327 ± 110	388 ± 32	42 ± 2	21 ± 1	this work
trans-[Ru(4-C≡$CC_6H_4NO_2$)Cl(dppm)$_2$] (**22**)	473 (1.8)	767	129			23
		770 ± 18	130 ± 3	40 ± 6	16 ± 3	this work
trans-[Ru{(*E*)-4,4′-C≡CC_6H_4CH=$CHC_6H_4NO_2$}Cl(dppm)$_2$] (**23**) (BB-II-154)	491 (2.6)	1964	235			23
		2120 ± 145	250 ± 17	150 ± 10	56 ± 4	this work
trans-[Ru(4,4′-C≡CC_6H_4C≡$CC_6H_4NO_2$)Cl(dppm)$_2$] (**24**)	466 (1.4)	833	161			20
				78 ± 4	33 ± 2	this work
trans-[Ru{(*E*)-4,4′,4″-C≡CC_6H_4C≡CC_6H_4CH=$CHC_6H_4NO_2$}Cl(dppm)$_2$] (**13**)	446 (1.1) (sh)	1825 ± 140	441 ± 34	46 ± 2	22 ± 1	this work
trans-[Ru{(*E*)-4,4′,4″-C≡CC_6H_4CH=CHC_6H_4C≡$CC_6H_4NO_2$}Cl(dppm)$_2$] (**15**)	452 (4.9)	2160 ± 66	495 ± 15	91 ± 4	41 ± 2	this work
trans-[Ru{(*E,E*)-4,4′,4″-C≡CC_6H_4CH=CHC_6H_4CH=$CHC_6H_4NO_2$}Cl(dppm)$_2$] (**17**)	466 (1.5)	2090 ± 66	395 ± 12	86 ± 5	36 ± 2	this work
trans-[Ru(4,4′,4″-C≡CC_6H_4C≡CC_6H_4C≡$CC_6H_4NO_2$)Cl(dppm)$_2$] (**25**)	439 (2.0)	1379	365			20

[a] Conditions: measurements were carried out in thf; all complexes are optically transparent at 1064 and 1300 nm. Errors ± 10% unless otherwise stated. [b] Corrected for resonance enhancement at 532 nm using the two-level model with $\beta_0 = \beta[1 - (2\lambda_{max}/1064)^2][1 - (\lambda_{max}/1064)^2]$. [c] Corrected for resonance enhancement at 650 nm using the two-level model with $\beta_0 = \beta[1 - (2\lambda_{max}/1300)^2][1 - (\lambda_{max}/1300)^2]$.

to the $Ru^{II/III}$ oxidation process in the range 0.49−0.74 V. It is noteworthy that the highest potentials correspond to **20** and **22** which are the two complexes possessing 4-nitrophenylethynyl ligands—the CVs of complexes with longer ligands display oxidation processes in the narrower range 0.49−0.60 V. Replacing yne linkage by an *E*-ene group at the phenylene adjacent to the metal center (proceeding from **19** to **21**, **24** to **23**, **18** to **14**, **12** to **16**, **13** to **17**, and **25** to **15**) leads to an increase in ease of metal-centered oxidation, but *E*-ene for yne replacement more remote from the metal center (proceeding from **18** to **12**, **14** to **16**, **25** to **13**, and **15** to **17**) leads to essentially no change in oxidation potential. Replacing dppe by dppm co-ligands results in most instances in a small increase in ease of oxidation. The cathodic behavior of these complexes is broadly similar. All show a reversible or quasi-reversible wave in the region −0.81 to −0.98 V, assigned to the nitro-centered reduction process, accompanied by a second and irreversible reduction process at about −1.10 V in the case of **20** and **22** (complexes containing the shortest alkynyl ligands). The nitro-centered reduction is easiest for the complexes with the 4-nitrophenylethynyl ligand (**20** and **22**).

Absorption maxima and intensities from electronic spectra are collected in Table 2. The intense low-energy bands in ruthenium alkynyl complexes of this type have been previously assigned as metal-to-ligand charge-transfer (MLCT) in character.[23] Intense low-energy transitions that result in significant changes in electron density distribution are important determinants of quadratic optical nonlinearity, so the optical absorption maxima and corresponding extinction coefficients for the MLCT bands in these complexes are potential indicators of their NLO merit. Developing an understanding of the effect on λ_{max} and ε of subtle changes in complex composition is clearly of importance. We have previously noted that π-chain lengthening by phenyleneethynylene units, in proceeding from **22** to **24** and then **25**, results in a progressive blue shift in absorption maximum,[20] at first glance a counter-intuitive trend; however, a similar trend is seen in the present work with the dppe-containing

(70) Hurst, S.; Lucas, N. T.; Cifuentes, M. P.; Humphrey, M. G.; Samoc, M.; Luther-Davies, B.; Asselberghs, I.; Van Boxel, R.; Persoons, A. *J. Organomet. Chem.* **2001**, *633*, 114.
(71) Hurst, S. K.; Humphrey, M. G.; Morrall, J. P.; Cifuentes, M. P.; Samoc, M.; Luther-Davies, B.; Heath, G. A.; Willis, A. C. *J. Organomet. Chem.* **2003**, *670*, 56.
(72) Long, N. J.; Martin, A. J.; White, A. J. P.; Williams, D. J.; Fontani, M.; Lashi, F.; Zanello, P. *J. Chem. Soc., Dalton Trans.* **2000**, 3387.
(73) Rigaut, S.; Perruchon, J.; Guesmi, S.; Fave, C.; Touchard, D.; Dixneuf, P. H. *Eur. J. Inorg. Chem.* **2005**, 447.
(74) Rigaut, S.; Massue, J.; Touchard, D.; Fillaut, J.-L.; Golhen, S.; Dixneuf, P. H. *Angew. Chem., Int. Ed.* **2002**, *41*, 4513.
(75) Samoc, M.; Gauthier, N.; Cifuentes, M. P.; Paul, F.; Lapinte, C.; Humphrey, M. G. *Angew. Chem., Int. Ed.* **2006**, *45*, 7376.

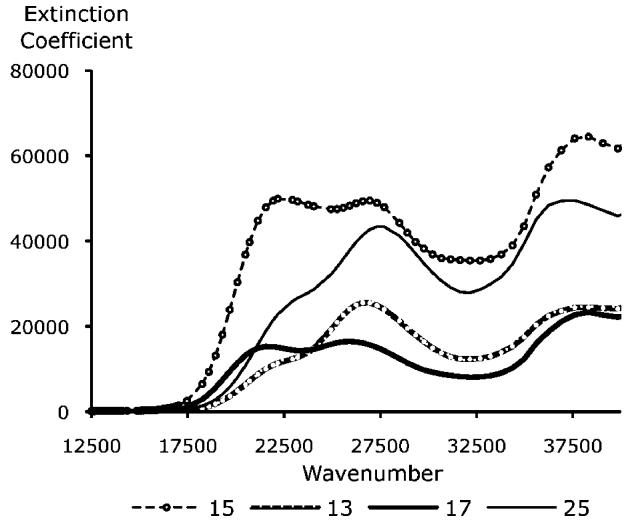

Figure 1. Optical spectra of *trans*-[Ru{(*E*)-4,4′,4″-C≡CC$_6$H$_4$C≡CC$_6$H$_4$CH=CHC$_6$H$_4$NO$_2$}Cl(dppm)$_2$](**13**),*trans*-[Ru{(*E*)-4,4′,4″-C≡CC$_6$H$_4$CH=CHC$_6$H$_4$C≡CC$_6$H$_4$NO$_2$}Cl(dppm)$_2$] (**15**), *trans*-[Ru{(*E,E*)-4,4′,4″-C≡CC$_6$H$_4$CH=CHC$_6$H$_4$CH=CHC$_6$H$_4$NO$_2$}Cl(dppm)$_2$] (**17**), and *trans*-[Ru(4,4′,4″-C≡CC$_6$H$_4$C≡CC$_6$H$_4$C≡CC$_6$H$_4$NO$_2$)Cl(dppm)$_2$] (**25**).

analogues, in proceeding from **20** to **19**, and then **18**. The systematically varied series of complexes listed in Table 2 enable additional structure−property observations to be made:

(i) related π-bridge lengthening by addition of phenyleneethynylene units, in proceeding from **21** to **14** or **23** to **15**, leads to a blue shift in λ_{max}.

(ii) π-bridge lengthening by phenyleneethenylene units in proceeding from **20** to **21** or **22** to **23** leads to a red-shift in λ_{max}, but a further lengthening by phenyleneethenylene, in proceeding from **21** to **16**, **19** to **12**, **23** to **17**, or **24** to **13**, leads to a blue shift in absorption maximum.

(iii) replacing yne-linkage with an *E*-ene linkage, in proceeding from **19** to **21**, **18** to **14**, **12** to **16**, **24** to **23**, **13** to **17**, **25** to **15**, **18** to **12**, **14** to **16**, **25** to **13**, or **15** to **17** results in a red-shift in λ_{max}.

(iv) there is little difference (maximum 10 nm) in λ_{max} between analogous dppm-containing and dppe-containing complexes.

(v) ε values for dppm/dppe complex pairs are similar, the one anomaly corresponding to the only complex for which the low-energy maximum is a shoulder (**13**).

(vi) in comparing the effect of varying alkynyl ligands, ε values are maximized with the **14**/**15** pair of complexes.

The effect on optical spectra of ene/yne exchange in the π-bridging unit in this series of complexes is illustrated in Figure 1. It is immediately apparent that the relative strengths of the two prominent low-energy bands are affected by the nature of the bridging unit. An *E*-ene linkage close to the metal center (**15**, **17**) results in the two bands having comparable intensities, whereas an yne linkage in the same position (**13**, **25**) results in the higher-energy band being significantly more intense. An yne linkage remote from the metal center (**15**, **25**) results in more intense bands overall compared to the case when an *E*-ene linkage is at the same site (**13**, **17**).

Theoretical Studies. TD-DFT calculations were undertaken to rationalize the linear optical spectra. Our TD-DFT calculations on the four model compounds delivered, for each model, the fifty lowest-energy symmetry-allowed single-photon transitions. Of this number, only a handful of calculated transitions for each model (all such transitions being of A′ symmetry for C_s-symmetric **12M**, **14M**, and **16M**, and of A_1 symmetry for C_{2v}-symmetric **18M**) have expectation values *f* greater than about 0.3 atomic units. It is these transitions which we expect to dominate the linear absorption spectra of compounds **12**−**19**.

The TD-DFT calculations reveal two different families of transitions as candidates for the observed λ_{max} values for **12**, **14**, **16**, and **18**. According to the PBE/TZP calculations (see Table 3), each of the model compounds **12M**, **14M**, **16M**, and **18M** exhibits two transitions of notably high expectation value *f*, in the windows 16500−17500 cm^{-1} and 22700−24000 cm^{-1}. The lower-energy of these transitions (^{3}A′ for **12M** and **16M**, ^{4}A′ for **14M**, $^3A_1$ for **18M**) is also characterized in the LB94/TZP calculations as having the largest *f* value among surveyed transitions: in the LB94/TZP calculations, this transition is identified as ^{3}A′ for the ethenyl-containing structures and $^3A_1$ for **18M**, with calculated transition energies at the LB94/TZP level of theory in the range 14100−15100 cm^{-1}. (Note that it is common for the transition energies determined using LB94/TZP to be systematically lower than the PBE/TZP values.) In contrast, the higher-energy of the notable PBE/TZP transitions (^{9}A′ for **12M**, ^{8}A′ for **14M** and **16M**, $^5A_1$ for **18M**) does not have a

(76) Li, Z.; Fehlner, T. P. *Inorg. Chem.* **2003**, *42*, 5715.
(77) Li, Z.; Beatty, A. M.; Fehlner, T. P. *Inorg. Chem.* **2003**, *42*, 5707.
(78) Qi, H.; Sharma, S.; Li, Z.; Snider, G. L.; Orlov, A. O.; Lent, C. S.; Fehlner, T. P. *J. Am. Chem. Soc.* **2003**, *125*, 15250.
(79) Qi, H.; Gupta, A.; Noll, B. C.; Snider, G. L.; Lu, Y.; Lent, C. S.; Fehlner, T. P. *J. Am. Chem. Soc.* **2005**, *127*, 15218.
(80) Cifuentes, M. P.; Powell, C. E.; Morrall, J. P.; McDonagh, A. M.; Lucas, N. T.; Humphrey, M. G.; Samoc, M.; Houbrechts, S.; Asselberghs, I.; Clays, K.; Persoons, A.; Isoshima, T. *J. Am. Chem. Soc.* **2006**, *126*, 10819.
(81) Rigaut, S.; Monnier, F.; Mousset, F.; Touchard, D.; Dixneuf, P. H. *Organometallics* **2002**, *21*, 2654.
(82) Hurst, S. K.; Cifuentes, M. P.; Humphrey, M. G. *Organometallics* **2002**, *21*, 2353.
(83) Hu, Q. Y.; Lu, W. X.; Tang, H. D.; Sung, H. H. Y.; Wen, T. B.; Williams, I. D.; Wong, G. K. L.; Lin, Z.; Jia, G. *Organometallics* **2005**, *24*, 3966.
(84) Klein, A.; Lavastre, O.; Fiedler, J. *Organometallics* **2006**, *25*, 635.
(85) Powell, C. E.; Hurst, S.; Morrall, J. P.; Cifuentes, M. P.; Roberts, R. L.; Samoc, M.; Humphrey, M. G. *Organometallics* **2007**, *26*, 4456.
(86) Younus, M.; Long, N. J.; Raithby, P. R.; Lewis, J.; Page, N. A.; White, A. J. P.; Williams, D. J.; Colbert, M. C. B.; Hodge, A. J.; Khan, M. S.; Parker, D. G. *J. Organomet. Chem.* **1999**, *578*, 198.
(87) Colbert, M. C. B.; Lewis, J.; Long, N. J.; Raithby, P. R.; White, A. J. P.; Williams, D. J. *J. Chem. Soc., Dalton Trans.* **1997**, 99.
(88) Jones, N. D.; Wolf, M. O. *Organometallics* **1997**, *16*, 1352.
(89) Lebreton, C.; Touchard, D.; Le Pichon, L.; Daridor, A.; Toupet, L.; Dixneuf, P. H. *Inorg, Chim. Acta* **1998**, *272*, 188.
(90) Choi, M.-Y.; Chan, M. C.-W.; Zhang, S.; Cheung, K.-K.; Che, C.-M.; Wong, K.-Y. *Organometallics* **1999**, *18*, 2074.
(91) Kim, B.; Beebe, J. M.; Olivier, C.; Rigaut, S.; Touchard, D.; Kushmerick, J. G.; Zhu, X.-Y.; Frisbie, C. D. *J. Phys. Chem. C* **2007**, *111*, 7521.
(92) Wong, C.-Y.; Che, C.-M.; Chan, M. C. W.; Han, J.; Leung, K.-H.; Phillips, D. L.; Wong, K.-Y.; Zhu, N. *J. Am. Chem. Soc.* **2005**, *127*, 13997.
(93) Onitsuka, K.; Ohara, N.; Takei, F.; Takahashi, S. *Organometallics* **2008**, *27*, 25.
(94) Olivier, C.; Kim, B.; Touchard, D.; Rigaut, S. *Organometallics* **2008**, *27*, 509.

Table 3. Computed Significantly-Allowed Single-Photon Transitions (Those with Oscillator Strengths Exceeding $f = 0.3$ a.u) for the Model Compounds **12M**, **14M**, **16M**, and **18M**, Obtained through PBE/TZP and LB94/TZP//PBE/TZP Calculations

		PBE/TZP						LB94/TZP					
species[a]	symm[b]	n[c]	E/eV[d]	f/a.u.[e]	occ.[f]	virt.[f]	wt %[g]	n[c]	E/eV[d]	f/a.u.[e]	occ.[f]	virt.[f]	wt %[g]
12M	A′	1	1.169	0.38	^{25}A″	^{26}A″	96	1	0.798	0.31	^{25}A″	^{26}A″	96
	A′	**3**	**2.089**	**0.70**	**^{25}A″**	**^{27}A″**	**87**	**3**	**1.778**	**0.56**	**^{25}A″**	**^{27}A″**	**87**
	A′	**9**	**2.917**	**0.95**	**^{24}A″**	**^{27}A″**	**59**	**6**	**2.512**	**0.53**	**^{24}A″**	**^{27}A″**	**46**
	A′	10	3.014	0.07	^{25}A″	^{30}A″	42	10	2.758	0.47	^{25}A″	^{30}A″	47
14M	A′	1	1.141	0.36	^{25}A″	^{26}A″	96	1	0.787	0.31	^{25}A″	^{26}A″	95
	A′	2	1.969	0.32	^{24}A″	^{26}A″	86	2	1.476	0.17	^{24}A″	^{26}A″	86
	A′	**4**	**2.114**	**0.90**	**^{25}A″**	**^{27}A″**	**85**	**3**	**1.834**	**0.84**	**^{25}A″**	**^{27}A″**	**68**
	A′							7	2.511	0.37	^{22}A″	^{26}A″	31
	A′	**8**	**2.878**	**0.84**	**^{24}A″**	**^{27}A″**	**46**						
	A′							10	2.696	0.38	^{25}A″	^{29}A″	35
16M	A′	1	1.196	0.44	^{25}A″	^{26}A″	94	1	0.848	0.34	^{25}A″	^{26}A″	94
	A′	2	2.020	0.42	^{24}A″	^{26}A″	81	2	1.556	0.21	^{24}A″	^{26}A″	81
	A′	**3**	**2.051**	**0.69**	**^{25}A″**	**^{27}A″**	**86**	**3**	**1.768**	**0.69**	**^{25}A″**	**^{27}A″**	**82**
	A′	**8**	**2.829**	**0.61**	**^{24}A″**	**^{27}A″**	**55**	**6**	**2.487**	**0.59**	**^{24}A″**	**^{27}A″**	**50**
	A′	13	3.107	0.46	^{25}A″	^{31}A″	69	13	2.882	0.16	^{25}A″	^{31}A″	67
18M	A_1	1	1.112	0.33	$^{17}B_2$	$^{18}B_2$	97	1	0.749	0.30	$^{17}B_2$	$^{18}B_2$	96
	A_1	**3**	**2.162**	**0.83**	**$^{17}B_2$**	**$^{19}B_2$**	**88**	**3**	**1.870**	**0.78**	**$^{17}B_2$**	**$^{19}B_2$**	**65**
	A_1	**5**	**2.975**	**1.01**	**$^{14}B_2$**	**$^{18}B_2$**	**42**	5	2.527	0.34	$^{14}B_2$	$^{18}B_2$	65
	A_1							**7**	**2.801**	**0.70**	**$^{17}B_2$**	**$^{20}B_2$**	**70**
	A_1							10	3.206	0.36	$^{15}B_2$	$^{19}B_2$	49

[a] Notation used for calculation on model compounds is consistent with that indicated in the main text. [b] Symmetry classification of the identified transition. [c] Energy ranking of the identified transition within the indicated symmetry classification. [d] Calculated transition energy in electron volts, at the indicated level of theory. [e] Calculated transition oscillator strength, in atomic units, at the indicated level of theory. [f] Principal pair of occupied and virtual orbitals involved in the identified transition. [g] Percentage contribution of principal-orbital character to the calculated transition, at the indicated level of theory.

prominent counterpart in the LB94/TZP calculations on **14M** and **18M**. The ^{6}A′ transitions for **12M** and **16M**, determined using LB94/TZP at an energy of ~20000 cm^{-1}, have the same principal character as the corresponding PBE/TZP ^{9}A′ (**12M**) or ^{8}A′ (**16M**) transitions. The strong $^5A_1$ feature determined for **18M** at the LB94/TZP level of theory, at an energy of ~22600 cm^{-1}, has no apparent counterpart in the calculated PBE/TZP spectrum.

For the ethenyl-containing models **12M**, **14M**, and **16M**, the most prominent transitions are consistently those of SLUMO ← HOMO and SLUMO ← SHOMO character, where SHOMO (^{24}A″ in each case) is an orbital whose principal character arises from π-bonding within the second and third C_2 units, HOMO (^{25}A″) exhibits π-bonding within the first C_2 unit (but with some leakage into the second C_2), and SLUMO (^{27}A″) displays cumulenic or diene-like character around the second (and, to a lesser degree, the third) C_2 unit. The LUMO itself (^{26}A″), which involves cumulenic or diene-like character around the third C_2 and phenylene-nitro C−N π-bonding, is important to some slightly less intense single-photon transitions. Orbital plots for the frontier orbitals of **12M** are displayed in Figure 2.

For **18M**, the lower-energy of the two prominent single-photon transitions is characterized as promotion from the acetylenic HOMO (dominated by electron density around the C≡C unit directly anchored to Ru, $^{17}B_2$) to the SLUMO $^{19}B_2$ which has cumulenic character focused around the second C≡C unit from Ru. Orbital plots for the orbitals implicated in this transition, and for the other strong transitions variously identified at the PBE/TZP and LB94/TZP levels of theory, are shown in Figure 3.

Spectroelectrochemical Studies. Selected examples were oxidized in an optically transparent thin-layer electrochemical (OTTLE) cell, the results being listed in Table 4, and a representative example being depicted in Figure 4. Oxidation using a potential of 0.8 V results in progressive replacement of spectral peaks corresponding to the starting compounds

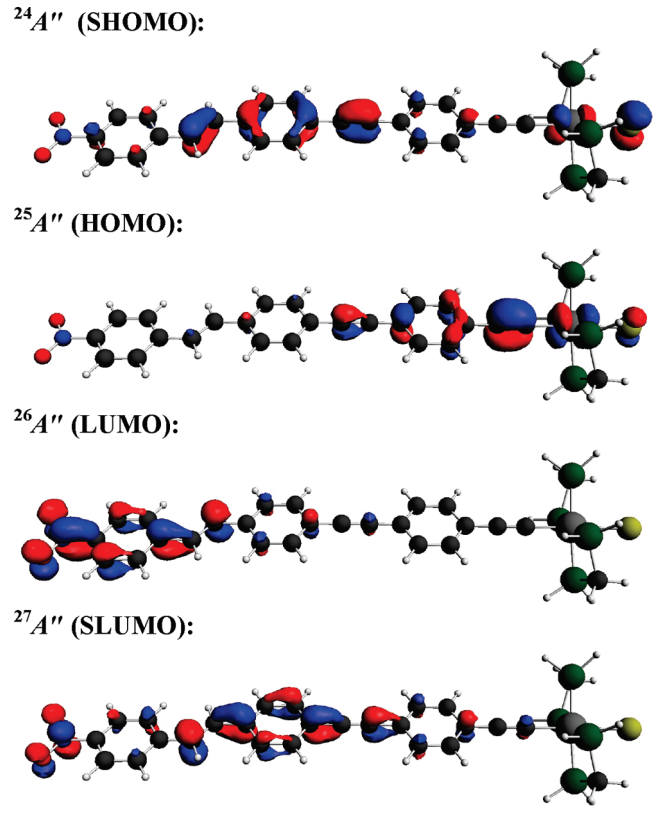

Figure 2. Orbital plots for the important frontier orbitals of model compound **12M**, calculated at the PBE/TZP level of theory. The frontier orbitals for models **14M** and **16M** are broadly similar in their composition, as described in the text. For all three ethenyl-containing models, the dominant symmetry-allowed single-photon transtions are those for which the principal occupied orbital is ^{24}A″ or ^{25}A″, and the principal virtual orbital is ^{27}A″.

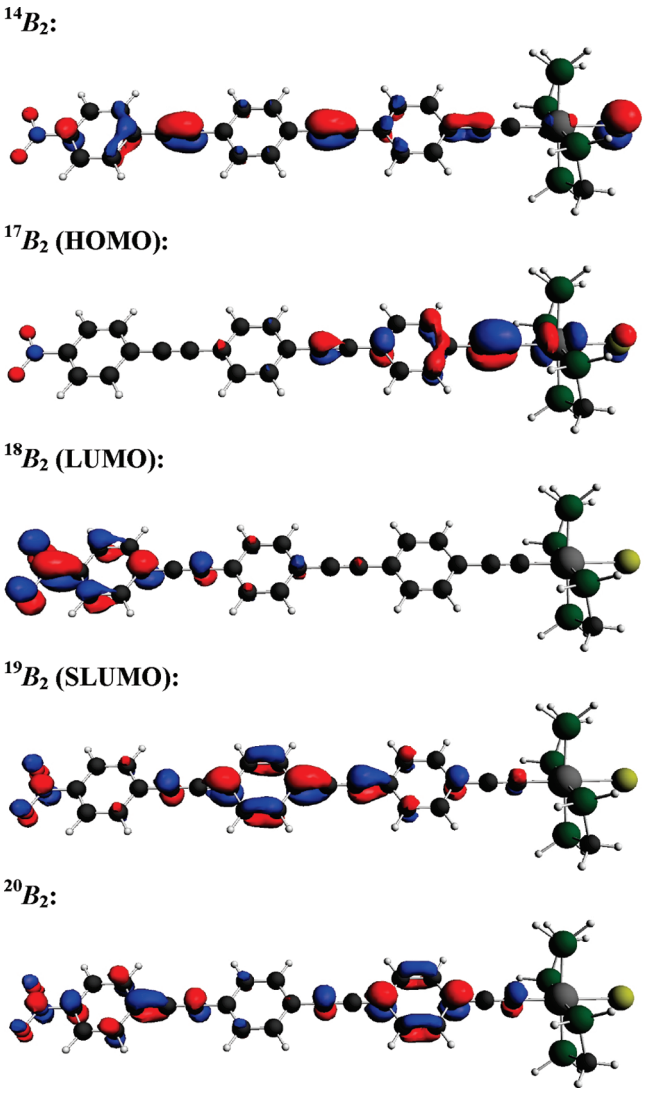

Figure 3. Orbital plots for the important frontier orbitals of model compound **18M**, calculated at the PBE/TZP level of theory. TD-DFT calculations at the PBE/TZP and the LB94/TZP levels of theory yield different results for the character of the important single-photon transitions for this species, as described in the text.

with those of the oxidized species, with isosbestic points in each case. We have previously reported the UV−vis−NIR spectral changes during electrochemical oxidation of *trans*-[Ru(C≡CR)Cl(dppe)$_2$] (R = Ph, C$_6$H$_4$−4-C≡CPh), which results in significant changes in the high-energy region, and appearance of new low-energy bands at 12035 cm^{-1} (R = Ph) and 11155 cm^{-1} (R = C$_6$H$_4$−4-C≡CPh).[13] This earlier study features complexes that lack a strong acceptor functionality. The present work examines complexes with an appended nitro substituent. Similar low-energy bands result on oxidation of **13**, **15**, **17**, and **25**, but in contrast to the earlier report, little change is observed in the high-energy region. The lowest-energy NIR bands are observed for complexes bearing an ethenyl group at the phenylethynyl ligated to the metal (**15**, **17**). We have previously demonstrated electrochemical switching of cubic NLO properties at the wavelengths corresponding to these low-energy bands;[11,13,14] the present complexes would similarly be expected to be prospective NLO molecular switches.

Quadratic Nonlinear Optical Studies. The quadratic nonlinearities of **12** to **25** have been determined at 1064 nm and (for most complexes) 1300 nm using the hyper-Rayleigh scattering technique; the results are presented in Table 2, together with the two-level-corrected values. We have discussed shortcomings with the two-level model in an earlier report;[20] although the two-level model is not generally considered adequate for donor-bridge-acceptor organometallic complexes such as those in the present study, it may have some utility in cases where the structural variation is restricted to the molecular components responsible for the low-energy charge-transfer bands in the linear optical spectrum. The low-energy bands for the present series of complexes are charge-transfer in nature and involve the alkynyl ligand that is the subject of systematic variation, so we have also explored the evolution of β_0 upon structural modification. Trends in β and β_0 for the 1064 nm data can be examined for the same compositional changes as those used to assess linear optical changes above, namely:

(i) π-bridge lengthening by addition of phenyleneethynylene groups, in proceeding from **20** to **19**, results in an increase in β, but further addition of C$_6$H$_4$C≡C in proceeding to **18** results in no further change; β_0 values increase monotonically for this structural modification.

(ii) π-bridge lengthening by addition of phenyleneethynylene units, in proceeding from **21** to **14** or **23** to **15**, leads (as in (i)) to no change (within error margins) in β, but an increase in β_0; both outcomes can be ascribed to the blue shift in λ_{max}, resulting in reduced resonance enhancement.

(iii) π-bridge lengthening by phenyleneethenylene units in proceeding from **20** to **21** or **22** to **23** leads to an increase in β and β_0 that mirrors the red-shift in λ_{max}. For other complexes, π-bridge lengthening by the first phenyleneethenylene, in proceeding from **19** to **12**, or **24** to **13**, leads to an increase in β and β_0 despite the blue shift in absorption maximum; for subsequent phenyleneethenylene addition (proceeding from **21** to **16** or **23** to **17**), β is invariant while β_0 increases, again the result of the blue shift in λ_{max}.

(iv) replacing yne-linkage with an *E*-ene linkage at the phenylene adjacent to the metal center, in proceeding from **19** to **21**, **18** to **14**, **12** to **16**, **24** to **23**, or **25** to **15**, results in an increase in β and β_0 accompanying the red-shift in λ_{max} (for the pair of complexes **13/17**, the outcome is less clear-cut, but there are difficulties in identifying the absorption maximum for the former). In contrast, *E*-ene for yne replacement more remote from the metal center (proceeding from **18** to **12**, **14** to **16**, or **15** to **17**) results in little change in β and a decrease in β_0.

(v) in most instances, there is an increase in β and β_0 upon replacing dppm by dppe co-ligands (proceeding from **23** to **21**, **24** to **19**, **15** to **14**, **17** to **16**, or **25** to **18**), although optical absorption maxima location and strength are similar.

(vi) in comparing the effect of varying alkynyl ligands, β values maximize with the same pair of complexes for which ε values are maximized (**14/15**).

Table 4. Cyclic Voltammetric[a] and Optical Data[b] for Selected Complexes and Their Oxidation Products

complex ([M])	$E_{1/2}$ [i_{pc}/i_{pa}], $Ru^{II/III}$	[M], ν_{max} [ε]	$[M]^+$, ν_{max} [ε]
trans-[Ru{(*E*)-4,4′,4″-C≡CC_6H_4C≡CC_6H_4CH=$CHC_6H_4NO_2$}Cl(dppm)$_2$] (**13**)	0.54 [1]	22400 sh [1.1]	11200 [0.79]
trans-[Ru{(*E*)-4,4′,4″-C≡CC_6H_4CH=CHC_6H_4C≡$CC_6H_4NO_2$}Cl(dppm)$_2$] (**15**)	0.49 [1]	22100 sh [4.9]	10300 [0.88]
trans-[Ru{(*E,E*)-4,4′,4″-C≡CC_6H_4CH=CHC_6H_4CH=$CHC_6H_4NO_2$}Cl(dppm)$_2$] (**17**)	0.49 [1]	21500 sh [1.5]	9700 [0.18], 10800 [0.16]
trans-[Ru(4,4′,4″-C≡CC_6H_4C≡CC_6H_4C≡$CC_6H_4NO_2$)Cl(dppm)$_2$] (**25**)	0.54 [1]	22800 sh [2.0]	11400 [0.81]

[a] CH_2Cl_2; Pt-wire auxiliary, Pt-working, and Ag/AgCl reference electrodes (ferrocene/ferrocenium couple located at 0.56 V); $E_{1/2}$ in V. [b] ν in cm^{-1}; [ε] in 10^4 M^{-1} cm^{-1}.

Table 5. Experimental Linear and Electric Field-Induced Second-Harmonic Generation-Derived Nonlinear Optical Response Parameters[a]

Complex	λ_{max} (nm), (ε, 10^4 cm^{-1})	$\mu\cdot\beta_{1907}$ (10^{-48} esu)	μ (10^{-18} esu)[b]	$\beta_{vec,1907}$ (10^{-30} esu)
trans-[Ru{(*E*)-4,4′-C≡CC_6H_4CH=$CHC_6H_4NO_2$}Cl(dppe)$_2$] (**21**)	489 (2.6)	590 ± 89	12.71	46 ± 12
trans-[Ru(4,4′-C≡CC_6H_4C≡$CC_6H_4NO_2$)Cl(dppe)$_2$] (**19**)	467 (1.8)	485 ± 73	12.94	37 ± 9
trans-[Ru{(*E*)-4,4′,4″-C≡CC_6H_4C≡CC_6H_4CH=$CHC_6H_4NO_2$}Cl(dppe)$_2$] (**12**)	448 (2.5)	780 ± 117	14.23	55 ± 14
trans-[Ru{(*E*)-4,4′,4″-C≡CC_6H_4CH=CHC_6H_4C≡$CC_6H_4NO_2$}Cl(dppe)$_2$] (**14**)	459 (3.5)	1009 ± 151	14.68	69 ± 17
trans-[Ru{(*E,E*)-4,4′,4″-C≡CC_6H_4CH=CHC_6H_4CH=$CHC_6H_4NO_2$}Cl(dppe)$_2$] (**16**)	459 (1.6)	865 ± 130	14.35	60 ± 15
trans-[Ru(4,4′,4″-C≡CC_6H_4C≡CC_6H_4C≡$CC_6H_4NO_2$)Cl(dppe)$_2$] (**18**)	433 (2.3)	910 ± 137	14.59	62 ± 15
trans-[Ru(4-C≡$CC_6H_4NO_2$)Cl(dppm)$_2$] (**22**)	473 (1.8)	348 ± 52	9.03	39 ± 10
trans-[Ru{(*E*)-4,4′-C≡CC_6H_4CH=$CHC_6H_4NO_2$}Cl(dppm)$_2$] (**23**)	490 (2.6)	610 ± 92	12.47	49 ± 12
trans-[Ru{(*E*)-4,4′,4″-C≡CC_6H_4C≡CC_6H_4CH=$CHC_6H_4NO_2$}Cl(dppm)$_2$] (**13**)	441 sh (1.1)	1190 ± 179	13.34	89 ± 22
trans-[Ru{(*E*)-4,4′,4″-C≡CC_6H_4CH=CHC_6H_4C≡$CC_6H_4NO_2$}Cl(dppm)$_2$] (**15**)	448 (4.9)	810 ± 122	14.00	58 ± 15
trans-[Ru{(*E,E*)-4,4′,4″-C≡CC_6H_4CH=CHC_6H_4CH=$CHC_6H_4NO_2$}Cl(dppm)$_2$] (**17**)	461 (1.5)	780 ± 117	14.27	55 ± 14
trans-[Ru(4,4′,4″-C≡CC_6H_4C≡CC_6H_4C≡$CC_6H_4NO_2$)Cl(dppm)$_2$] (**25**)	439 (2.0)	1060 ± 159	13.74	77 ± 19

[a] Conditions: measurements were carried out in $CHCl_3$; all complexes are optically transparent at 1907 and 959 nm. [b] Calculated for PH_2-containing models of the indicated compounds, at the PBE/TZP level of theory, using ADF2004. An uncertainty of ±10% is ascribed to the calculated dipole moments.

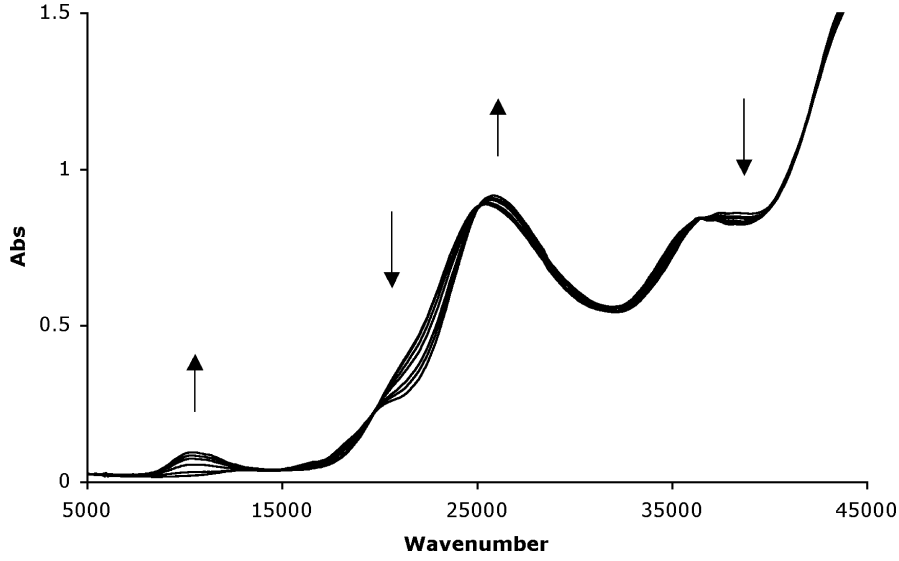

Figure 4. UV−vis−NIR spectral changes during the electrochemical oxidation of *trans*-[Ru{(*E*)-4,4′,4″-C≡CC_6H_4CH=CHC_6H_4C≡$CC_6H_4NO_2$}Cl(dppm)$_2$] (**15**).

Some of the results at 1300 nm are puzzling: increasing π-bridge length (proceeding from **21/23** to **14/15** or **16/17**, or from **19** to **18**) results in a decrease in nonlinearity, and indeed the largest β_{1300} (and corresponding β_0) values are found for the **21/23** pair of complexes. The lack of correspondence in β_0 values from HRS measurements at the two wavelengths is consistent with a lack of applicability of the two-level model for this class of complex.

Table 5 contains EFISH-derived $\mu\cdot\beta$ products for selected complexes at 1907 nm, β values at this wavelength assuming calculated dipole moments obtained from theoretical studies. While there is no consistent variation in β value arising from replacement of yne linkage by ene linkage or co-ligand dppm by dppe across this series of complexes, π-system lengthening is clearly important; the smallest β_{EFISH} values are found with complexes bearing the shorter alkynyl ligands (**19**, **21**−**23**).

Discussion

The present studies have afforded a range of alkynylruthenium complexes that can also be viewed as systematically varied hybrid OPE/OPV trimers end-capped with ligated metal and nitro groups. This suite of compounds has permitted assessment of the effect of a number of molecular modifications on electrochemical, linear, and nonlinear optical properties. For example, co-ligand variation at the metal (replacing dppe by dppm) results in a small increase in the potential of metal-centered oxidation, an insignificant difference in optical absorption maximum, and no change or a small decrease in HRS-derived β and β_0 values at 1064 nm. We have not probed this modification theoretically, but introduction of extra methylene units into the strap of the diphosphine ligands would be expected to increase their electron-donating capacity

slightly; a small increase in E^0_{ox} on proceeding from dppe-containing complex to dppm-containing analogue might therefore be anticipated, consistent with observation.

Replacing yne linkage with *E*-ene group at the phenylene adjacent to the metal center results in an increase in ease of metal-centered oxidation, a red-shift in λ_{max}, and an increase in β and β_0 at 1064 nm; a similar structural change remote from the metal leads to a red-shift in λ_{max}, but no change in oxidation potential, β, or β_0 value. Our calculations suggest that the HOMO is localized at the ligated Ru and immediately adjacent phenylethynyl unit, so it is understandable that linkage modification at this adjacent ring results in a change in metal-centered-oxidation potential, but that similar modifications remote from the metal center have lesser or no impact. While replacement of yne by ene linkage results in a red-shift in λ_{max} if this modification occurs at the ring adjacent to the metal center or remote from the metal, the magnitude of the red shift is considerably greater for the former. The calculations suggest that the crucial low-energy band is SLUMO ← HOMO in character in all cases (Table 3). The HOMOs contain a contribution from the C_2 unit attached to the phenyl adjacent to the metal center but not from that linking the "middle" ring to the nitro-containing ring. Similarly, the SLUMOs have a greater contribution from the "middle" C_2 unit than from the nitrophenyl-attached C_2. The far greater contribution of the "middle" C_2 unit to the crucial orbitals responsible for the low-energy bands is consistent with modifications at this linkage having a greater impact on these bands. The decreased influence on linear optical properties is reflected in a diminished change in quadratic nonlinear optical properties upon this structural modification.

π-Bridge lengthening by phenyleneethenylene units results in an increase in ease of metal-centered oxidation, and a red-shift in λ_{max} in proceeding to 4-nitrophenyl-(*E*)-ethenylphenylethynyl complexes, but a blue-shift for this structural change more remote from the metal center. Although we have not explored this structural modification theoretically, our calculations consistently show that the HOMO is localized at the ligated Ru and adjacent phenyleneethynyl unit in complexes of this type (see Figures 2 and 3). One would therefore expect that the influence of the electron-withdrawing nitro group on E^0_{ox} would greatly diminish on proceeding from **20** or **22** to the longer chain complexes **21** or **23**, respectively, and that further π-system lengthening in proceeding to **16** or **17** would have even less effect on this parameter. The increased remoteness of the nitro group from the crucial phenyleneethynylruthenium unit (proceeding from **20** to **21** or **22** to **23**) is expected to destabilize the HOMO, and thereby red-shift λ_{max}, as is observed. [This is expected because this band has been assigned theoretically as SLOMO ← HOMO in character. Because the calculations suggest that the most important transitions (SLUMO ← HOMO and SLUMO ← SHOMO) are predominantly metal-to-bridge charge-transfer in character (Figure 2), the nitro group is not considered to influence λ_{max} to a significant extent.] The blue-shift in λ_{max} observed on further π-system lengthening (proceeding to **16** or **17**, respectively) is at first glance counter-intuitive but may reflect an increasingly important twisting out of coplanarity of the extended π-bridge. Consistent with this idea, the β values increase markedly on proceeding from **20** to **21** or **22** to **23**, but do not increase further on proceeding to **16** or **17**, respectively. The β_0 values are an approximation for removal of the resonance enhancement that becomes increasingly important as λ_{max} approaches the wavelength corresponding to the second-harmonic of the incident laser (532 nm in the present study). The β_0 data reveal a consistent increase on bridge lengthening, indicating that any loss of coplanarity does not affect the bridge-length dependent increase in β_0.

The present results suggest that optimizing nonlinearity in this system can be achieved by employing dppe co-ligands, and lengthening the π-system by ene-linkage rather than yne-linkage, the latter a similar structure−property outcome to that in the purely organic domain. However, because the impact of yne for ene replacement is greatest at the first bridging C_2 unit, and diminishes thereafter, the choice of NLO-active target may well be dictated by chemical synthesis considerations. Our TD-DFT calculations reveal that the "remote" ene for yne structural modification has little effect on the nature of the crucial frontier molecular orbitals once one ene-linkage is in place. Note, though, that for the "all-yne-linked" complex, the HOMO and LUMO have a similar composition to complexes with ene-linkages, but with the nitrophenyl contribution to the SLUMO decreased, which impacts on both linear and nonlinear optical properties.

Three further observations can be made. First, the smaller data sets for $\beta_{1300,HRS}$ and $\beta_{1907,EFISH}$ have not afforded structure−property outcomes with the same clarity, although the expected π-bridge length-nonlinearity dependence has been noted. Second, the lack of correspondence of β_0 values calculated for data at different wavelengths highlights shortcomings in the two-level model. Finally, the appearance of low-energy bands of moderate intensity in the NIR region for the oxidation products of **13**, **15**, **17**, and **25** suggests that these complexes may show a similar potential for electrochemical switching of cubic nonlinearity to that already demonstrated with complexes possessing a shorter π-bridge.

Acknowledgment. We thank the Australian Research Council (M.G.H., R.S.), the Fund for Scientific Research-Flanders (FWO-Vlaanderen; FWO0297.04) (K.C.), and the Katholieke Universiteit Leuven (GOA/2006/03) (K.C.) for support of this work. M.G.H. is an ARC Australian Professorial Fellow and R.L.R. was an ARC International Fellow. B.B. thanks King Abdulaziz University for sponsorship.

Supporting Information Available: List of authors of ref 43, the syntheses of compounds **1**−**11** and complexes **13**−**19**. This material is available free of charge via the Internet at http://pubs.acs.org.

IC801953Z